Solving the spatially dependent Boltzmann's equation for the electron-velocity distribution using flux corrected transport

John V. DiCarlo[a] and Mark J. Kushner[b]
University of Illinois, Department of Electrical and Computer Engineering, Gaseous Electronics Laboratory, 607 East Healey, Champaign, Illinois 61820

(Received 10 July 1989; accepted for publication 6 September 1989)

Boltzmann's equation (BE) for the electron-velocity distribution (EVD) in partially ionized plasmas is not usually directly integrated as an initial value problem using finite differences. This circumstance is a result of numerical effects which blur sharp density boundaries in the position-velocity plane. To address this issue, we have applied flux corrected transport (FCT) to solving BE and demonstrated the method by calculating the EVD in the cathode fall of a He glow discharge by direct integration. Unidirectional and bidirectional EVDs are considered, and comparisons are made to conventional multibeam and Monte Carlo simulations to validate our method. We find that using FCT to solve BE is a significant improvement over conventional finite difference methods, being both more accurate and computationally faster.

I. INTRODUCTION

Obtaining an accurate representation of the electron-velocity distribution (EVD) in low-temperature plasmas is of paramount importance if one is to accurately calculate electron transport coefficients. This is particularly important under conditions where the EVD is not in equilibrium with the local electric field. This condition occurs if the rate of energy or momentum relaxation ν_e or the distance over which the EVD equilibrates λ is small compared to the rate of change of the electric field,

$$\nu_e < \frac{1}{E}\frac{\partial E}{\partial t} \quad \text{or} \quad \frac{1}{\lambda} < \frac{1}{E}\frac{\partial E}{\partial x}. \tag{1}$$

These conditions are usually found in the cathode fall of glow discharges[1-3] and in high-frequency (> MHz) low-pressure discharges as used in plasma processing.[4-6] The typical time and distance required for the EVD to come into equilibrium with an applied electric field is shown in Fig. 1 for electron swarms in Ar and N_2. These results were obtained by applying a step function in electric field to a thermal (0.05 eV) electron distribution and observing the time or distance required for the EVD to reach the steady state. In low-pressure argon plasmas (< a few Torr) and moderate electric fields ($\simeq$10–100 Townsends (Td), 1 Td = 10^{-17} V cm^2) the equilibration time and distance are 10–100 ns and 0.1–1.0 cm. Under these conditions spatial and/or temporal development of the EVD must be considered.

The temporal and spatially dependent EVD is obtained from solution of Boltzmann's equation (BE),

$$\frac{\partial f}{\partial t}(\mathbf{v},\mathbf{r},t) = -\mathbf{v}\cdot\nabla_{\mathbf{r}} f - \mathbf{a}\cdot\nabla_{\mathbf{v}} f + \left(\frac{\partial f}{\partial t}\right)_c, \tag{2}$$

where the $f(\mathbf{v},\mathbf{r},t)$ is the electron velocity distribution. The terms in Eq. (2) represent the change in the EVD due to convection in coordinate space with velocity $\mathbf{v}$, convection in velocity space with acceleration $\mathbf{a}$, and changes in the EVD due to collisions. For electrons in an unmagnetized glow discharge, $\mathbf{a} = -e\mathbf{E}(\mathbf{r},t)/m_e$, where E is the local instantaneous electric field and m_e is the electron mass. Transport coefficients, such as the rate constant for electron impact ionization of neutrals $k_I(\mathbf{r},t)$ (cm^3/s), are obtained by convolving the EVD with the electron impact cross section and velocity

$$k_I(\mathbf{r},t) = \int_0^\infty f(\mathbf{v},\mathbf{r},t)|\mathbf{v}|\sigma(|\mathbf{v}|)d^3v. \tag{3}$$

Solving BE under nonequilibrium conditions for analysis of low-temperature partially ionized plasmas has been the topic of many previous works.[7-11] For example, BE is commonly solved using a spherical harmonic expansion, $f(\mathbf{v},t) = \Sigma_i f_i(v,t)P_i[\cos(\theta)]$, where P_i is the Legendre polynomical and θ is measured with respect to the applied electric field.[7] This method may, however, require many terms in order to correctly include the effects of anisotropic scattering,[8] and is not easily extended to multiple spatial dimensions. Beam solutions for BE are convenient in regions of rapidly changing electric fields such as in the cathode fall of a glow discharge.[10,11] Beam solutions are poor, however, at

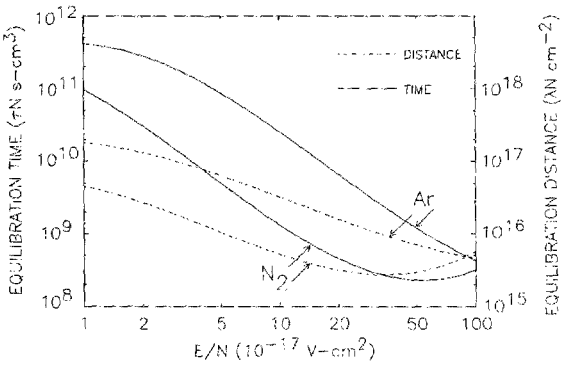

FIG. 1. Approximate times and distances required for an electron velocity distribution to come into equilibrium with a step function in electric field for swarms in Ar and N_2. The quantities have been normalized by gas density.

[a] Present address: Kennedy School of Government, Harvard University, Cambridge, MA.
[b] Author to whom correspondence should be addressed.

 0021-8979/89/245763-12$02.40

correctly treating nonforward scattering, and time-varying electric fields are difficult to account for. A recent improvement to the beam method, using a convective propagator, alleviates many of those restrictions.[12] Finally, Monte Carlo particle simulations abandon solutions of BE in favor of directly integrating the equations of motion of individual particles, and in doing so yield an exact representation of the EVD.[1,6,13]

In very few cases is BE, a first-order partial differential equation, solved by direct integration as a boundary value or initial value problem using finite differences.[9] This condition arises primarily because of the effects of numerical inaccuracies, such as numerical diffusion, which blur sharp boundaries in the energy-position (ϵ,x) plane. This is particularly important with respect to computing excitation rates for processes which have threshold energies. For example, in the cathode fall of an electric discharge the electric potential $\phi(x)$ changes rapidly as a function of distance from the cathode.[2,14,15] Ignoring superelastic collisions and electrons emitted from the cathode with significant energy, electrons are excluded from that position of the (ϵ,x) plane which has higher energies than $e\phi(x)$. If low-order finite difference techniques are used to integrate BE, such as the donor cell method, significant numerical diffusion may result. As a consequence, the cited sharp boundary in the (ϵ,x) is blurred and electron density may be placed in the excluded region [that is, in the plane to the left of $e\phi(x)$]. Such a solution for $f(\mathbf{v},x)$ will therefore predict electron impact rate constants $k(x)$ for processes having threshold energies at spatial locations closer to the cathode than energetically allowed. Integrating BE using higher-order differencing methods may preserve sharp boundaries in the (ϵ,x) plane, however they may also introduce unphysical ripples. These ripples may lead to instabilities since the local rate of ionization is increased by the magnitude of the ripple, which further increases the local rate of ionization.

If the spread, or numerical diffusion, of a beam in the electron distribution in *energy space* is symmetric about its mean value ϵ_0, then energy is conserved since the integral of $f(\epsilon)$ in the vicinity of ϵ_0 still yields the mean value. If a collision cross section has a near constant value in the vicinity around ϵ_0, then the resulting rate constant should also be conserved. If, however, numerical diffusion occurs in velocity space, energy conservation is not guaranteed since there is a fractional residual in the mean energy, for a Gaussian spread about V_0, proportional to $(\Delta v/V_0)^2$. Therefore limiting numerical diffusion, that is minimizing Δv, in such cases is important not only with respect to obtaining rate coefficients but also with respect to conserving energy.

The problem we have described of preserving sharp gradients in convective transport is not unique and many integration methods have been developed to deal with it. We may take advantage of those techniques to directly integrate BE as an initial value problem by noting the similarity between the two divergent terms in BE. The first term, $-\mathbf{v}\cdot\nabla_x f$, is the usual convective transport term in coordinate space. The second divergent term in BE, $-\mathbf{a}\cdot\nabla_v f$, can be viewed of as convection in velocity space driven by the acceleration. In doing so integration methods developed for conventional convective transport may be adapted to solve BE. The n-dimensional, time-dependent BE is simply solved as an initial value problem for convection in $2n$ dimensions; n dimensions for coordinate space and n dimensions for velocity space.

In this paper, we introduce the concept of using flux corrected transport (FCT) for directly integrating Boltzmann's equation for the EVD using finite differences. FCT is a conservative method for integrating convective transport equations using finite difference equations which is capable of preserving steep gradients in the solution while eliminating the ripple associated with higher-order solutions.[16-22] This is precisely the requirement that must be met to preserve the boundary of exclusion in the (ϵ,x) plane when solving BE as an initial value problem by direct integration. FCT has previously been successfully used to integrate the moments of BE equation (continuity, momentum) to simulate streamer propagation.[23-25] The innovation we propose is to use FCT to directly solve BE.

In Sec. II, we will briefly describe the basis of the FCT algorithms and in Sec. III we will discuss our particular application of FCT to solving BE. As a demonstration of the method, we solved for $f(\mathbf{v},x)$ in the cathode fall of a glow discharge in He. This solution is presented in Sec. IV where comparisons are also made to multibeam and Monte Carlo solutions for the same conditions to validate our method. Concluding remarks are in Sec. V.

II. OVERVIEW OF THE FLUX CORRECTED TRANSPORT ALGORITHMS

Flux corrected transport (FCT) is a numerical technique developed by Boris and Book[16] for integrating partial differential equations using finite differences. The FCT method possesses the advantages of both high- and low-order finite difference schemes. Like low-order schemes, FCT does not produce the dispersive ripples that higher-order schemes do. Like higher-order schemes, FCT does not suffer from the low accuracy and excessive numerical diffusion which are characteristic of low-order schemes. The key feature of FCT is the use of a corrective diffusion which is localized in only those regions where nonphysical ripples tend to form due to dispersion (i.e., in the neighborhood of steep gradients) and smooths those ripples. The corrective diffusive flux is nonlinear, as its magnitude depends on the values of the dependent variable from point to point, and is implemented in a conservative fashion. The diffusive flux is canceled by an opposite antidiffusive flux where the diffusion is clearly not needed. The operation which determines how much of the diffusive flux is canceled is called flux correction or flux limiting.

The algorithm for applying FCT to convective transport will be briefly described. Consider the continuity equation

$$\frac{\partial f}{\partial t}+\frac{\partial}{\partial x}(fv)=0, \tag{4}$$

where f is a density and v is the convective velocity. A finite difference solution to this equation is in conservative form when it can be written as

$$f_i^{n+1} = f_i^n - \frac{\Delta t}{\Delta x_i}(F_{i+1/2} - F_{i-1/2}), \tag{5}$$

where f_i^n is the density at location x_i and time t_n. $F_{i+1/2}$ is the flux of f at the boundary between numerical cell i and cell $i+1$. The time step is $\Delta t = t_{n+1} - t_n$ and $\Delta x_i = x_{i+1/2} - x_{i-1/2}$, which are the boundaries of the cell. The dependence of F (the transported fluxes) on f defines the integration scheme. Some common examples are leap-frog, Lax–Wendroff, Crank–Nicholson, and donor cell. The general sequence of the FCT algorithm is as follows[17,18]:

(i) Compute $F^L_{i+1/2}$, the transportive flux, using a low-order scheme (denoted by the superscript L) which is guaranteed to give ripple-free results.

(ii) Compute the updated transported and diffused[16] low-order solution for f, denoted by f^{td}, using F^L,

$$f_i^{td} = f_i^n - \frac{\Delta t}{\Delta x_i}(F^L_{i+1/2} - F^L_{i-1/2}). \tag{6}$$

(iii) Compute $F^H_{i+1/2}$, the transportive flux using a high-order scheme (denoted by the superscript H) which will preserve the steep boundaries of interest.

(iv) Define the antidiffusive flux. This is generally performed by one of two methods. The first is to take the antidiffusive flux to be the difference between the high- and low-order transportive fluxes,[17]

$$A_{i+1/2} = F^H_{i+1/2} - F^L_{i+1/2}. \tag{7}$$

The second method is to assume the form

$$A_{i+1/2} = \mu_{i+1/2}(f^{td}_{i+1} - f^{td}_i), \tag{8}$$

where $\mu_{i+1/2}$ is an antidiffusion coefficient which is determined by performing a Fourier analysis on the full update sequence and minimizing the amplitude and phase errors.[19] This is the method used in this work.

(v) Limit the antidiffusive fluxes $A_{i+1/2}$ in such a manner such the f^{n+1} as computed in (vi) are free of extrema not found in f^{td} or f^n,

$$A^c_{i+1/2} = C_{i+1/2}A_{i+1/2}, \quad 0 \leqslant C_{i+1/2} \leqslant 1. \tag{9}$$

(vi) Finally, apply the limited antidiffusive fluxes,

$$f_i^{n+1} = f_i^{td} - \frac{\Delta t}{\Delta x_i}(A^c_{i+1/2} - A^c_{i-1/2}). \tag{10}$$

The critical juncture in this method is step (v), as without flux limiting, f_i^{n+1} would simply be the time-advanced high-order solution. Note that since steps (i) and (ii) give a low-order update, steps (iii)–(vi) can be added as an enhancement to an existing low-order finite difference algorithm.[20]

The critical flux-limiting step described above bounds the antidiffusive fluxes so that they do not generate new maxima or minima in the solution, nor accentuate already existing extrema. This step is the poorest defined in the FCT algorithm and many methods have been proposed to select the antidiffusive fluxes and the flux limiters. Errors can arise in this step if the flux limiter overcorrects the antidiffusive fluxes and leaves an unnecessarily large net diffusion. These errors result in clipping of peaks and filling of troughs. Boris and Book's[16] original limiter is computationally fast, but tends to clip peaks. This limiter applies the criterion that the antidiffusive fluxes do not generate new maxima or minima in the transported and diffused solution. Thus, for a peaked density profile, diffusion in the low-order transport and diffuse step causes the peak in f^{td} to be smaller than the peak in f^n, leaving the limiter with no information to resurrect the original peak. After successive application of this limiter, a triangle profile develops a flattop. Because the limiter assumes a worst case, this is classified as being a strong flux correction.[18]

A more general flux limiter, given by Zalesak,[17] sets a maximum and a minimum density at each grid point and limits the antidiffusive fluxes so that the updated values do not exceed these bounds. Any physically motivated upper and lower bound on f_i^{n+1} can be used. One prescription proposed by Zalesak is to examine not only f^{td} at location i, and neighboring points at locations $i-1$ and $i+1$, but also to use f_i^n and its neighbors to determine the maximum and minimum values for f_i^{n+1}. For peaked profiles, this limiter remembers the value of the peak before it was reduced by the transport and diffuse step, and is able to resurrect it at each time step.

A very useful variation of the flux limiters described above is one-sided flux limiting. In this method, for example, maxima are allowed to appear or grow while minima are restricted as before. If mass is shifted from a mesh point to its neighbor, the density of the latter increases while the density of the former decreases, thereby creating a local minimum. Therefore, preventing the formation of minima forces some measure of control on the formation or enhancement of maxima. Using one-sided limiters results in profiles where only the troughs can be clipped. The choice of flux limiters depends on the physics of the problem at hand, and on the numerical properties of the integration scheme. For example, an integration scheme with very diffusive transport may work well with a permissive flux limiter, whereas a more dispersive algorithm may require strong flux correction.

III. APPLICATION OF FCT TO THE SOLUTION OF BOLTZMANN'S EQUATION

In this section our application of flux corrected transport to the solution of Boltzmann's equation is described. As a demonstration of the method, we have solved the one-dimensional BE in the cathode fall of a glow discharge while accounting for nonforward scattering. In doing so, we can compare our method to conventional solutions of BE for the same conditions as a validation procedure. The electric field in the cathode fall scales as $E(x) = (2V_c/d_c)(1 - x/d_c)$, where V_c is the cathode fall voltage, d_c the fall thickness, and x is the distance from the cathode.[2,14,15] For typical conditions, $E/N \lesssim 500$–1000 Td ($1\ \text{Td} = 10^{-17}\ \text{V cm}^2$) in the cathode fall. In low-pressure ($<$ a few Torr) discharges, these values are highly nonequilibrium, and therefore a stringent test of the method.

A. Electron transport

We solved the one-dimensional Boltzmann's equation [Eq. (1)] to obtain the electron velocity distribution $f(v_x,x,t)$ having the following independent variables; x is the

distance from the cathode, v_x is the velocity in the x direction; and t is the time. Spatial transport in one dimension was solved using FCT as described in Sec. II. The transport in velocity space is completely analogous to that in coordinate space, and was solved using identical algorithms. The dual convection was handled using a time-splitting procedure. After performing an update in coordinate space for time-step Δt, an update was performed in velocity space over the same Δt to complete the transport step. The time step was chosen to be half the Courant[26] value determined from both the spatial and velocity meshes. The time-splitting procedure is not a requirement of the FCT method as fully two-dimensional algorithms are available.[17,24,25] As a test we implemented both time splitting and full two-dimensional algorithms and found no significant differences between them for our conditions. We therefore used the time-splitting technique, which is simpler and computationally faster than the fully multidimensional approach.[22] In solving Boltzmann's equation in the cathode fall, a nonuniform computational mesh was used. The x_i's were placed at points corresponding to a fixed change in potential in order to resolve the high field region near the cathode. The v_j's were spaced evenly from zero velocity up to one third the maximum velocity as given by the cathode fall voltage. The remainder of the v_j's were placed so that the corresponding energy intervals were uniformly spaced.

Since the emphasis of this work is on developing methods for applying FCT to integrating BE under nonequilibrium conditions, three different transport algorithms were investigated. These transport algorithms are the donor cell method (DCM), sharp and smooth transport algorithm (SHASTA), and SHASTA low-phase error (LPE). In discussing these algorithms, we will only discuss the update in coordinate space. The update in velocity space is completely analogous to that in coordinate space.

The first algorithm uses the DCM for the low-order transport and diffuse step,[20]

$$f_{i,j}^{\mathrm{td}} = f_{i,j}^{n} - \frac{\Delta t}{\Delta x_i}(F_{i+1/2,j}^{L} - F_{i-1/2,j}^{L}), \tag{11}$$

where $f_{i,j}^{n}$ refers to the velocity distribution at position x_i, velocity v_j, and time-step n. The low-order transportive flux is

$$F_{i+1/2,j}^{L} = f_{i,j} v_j \quad \text{for } v_j \geqslant 0 \tag{12a}$$

$$= f_{i+1,j} v_j \quad \text{for } v_j < 0. \tag{12b}$$

The antidiffusive fluxes we used are those given by Boris and Book[20] but generalized for use on a nonuniform grid,

$$A_{i+1/2,j} = \mu_{i+1/2,j}(f_{i+1,j}^{\mathrm{td}} - f_{i,j}^{\mathrm{td}}), \tag{13}$$

where

$$\mu_{i+1/2,j} = (1/2)\epsilon_{i+1/2,j}(1 - \epsilon_{i+1/2,j}), \tag{14a}$$

$$\epsilon_{i+1/2,j} = (v_j \Delta t)/(x_{i+1} - x_i). \tag{14b}$$

The flux limiter which we used is the one-sided variant of that proposed by Zalesak.[17] First, the minimum value that $f_{i,j}$ can be reduced to by the antidiffusive fluxes is determined,

$$f_{i,j}^{b} = \min(f_{i,j}^{n}, f_{i,j}^{\mathrm{td}}), \tag{15a}$$

$$f_{i,j}^{\min} = \min(f_{i-1,j}^{b}, f_{i,j}^{b}, f_{i+1,j}^{b}). \tag{15b}$$

Next, the sum of all antidiffusive fluxes away from grid point i is calculated,

$$P_{i,j}^{+} = \max(0, A_{i+1/2,j}) - \min(0, A_{i-1/2,j}). \tag{16}$$

Then the least upper bound on the fraction which must multiply all antidiffusive fluxes away from grid point i to guarantee no undershoot of $f_{i,j}$ at grid point i is determined,

$$R_{i,j}^{+} = \begin{cases} \min(1, (f_{i,j}^{\mathrm{td}} - f_{i,j}^{\min})\Delta x_i / P_{i,j}^{+}) & \text{if } P_{i,j}^{+} > 0 \\ 0 \quad \text{if } P_{i,j}^{+} = 0. \end{cases} \tag{17}$$

Then the antidiffusive fluxes are limited,

$$A_{i+1/2,j}^{c} = A_{i+1/2,j} R_{i,j}^{+} \quad \text{if } A_{i+1/2,j} \geqslant 0, \tag{18a}$$

$$= A_{i+1/2,j} R_{i+1,j}^{+} \quad \text{if } A_{i+1/2,j} < 0. \tag{18b}$$

Finally, the corrected antidiffusive fluxes are applied,

$$f_{i,j}^{n+1} = f_{i,j}^{\mathrm{td}} - \frac{\Delta t}{\Delta x_i}(A_{i+1/2,j}^{c} - A_{i-1/2,j}^{c}). \tag{19}$$

The analogous steps in velocity space are then performed, thus completing the transport update for one time step.

The second and third methods investigated in this work use the sharp and SHASTA and Pheonical SHASTA LPE algorithms of Boris and Book.[18] These algorithms were used for the transport and diffuse step, and for the antidiffusive fluxes. The expressions we used had been generalized for use on a nonuniform mesh by Morrow and Cram.[21] SHASTA uses the following for the low-order fluxes:

$$P_{i+1/2}^{L} = (x_{i+1} - x_i)\{\epsilon_{i+1/2,j}[(f_{i,j}^{n} + f_{i+1,j}^{n})/2] + v_{i+1/2}(f_{i+1,j}^{n} - f_{i,j}^{n})\}, \tag{20}$$

where

$$v_{i+1/2,j} = \tfrac{1}{8} + \tfrac{1}{2}\epsilon_{i+1/2,j}^{2}, \tag{21}$$

and $\epsilon_{i+1/2,j}$ is given by Eq. (14b). Here v can be thought of as a diffusion coefficient and the terms in Eq. (20) having v are the added diffusion which will be removed by the flux limiter when it is not needed. The antidiffusion fluxes in the SHASTA algorithm are the same as that for the DCM [Eq. (13)] with $\mu_{i+1/2,j} = \frac{1}{8}$. The SHASTA algorithm also used the same flux limiter as the DCM, which is given by Eqs. (15)–(18).

The Pheonical SHASTA LPE algorithm is similar to the SHASTA method but can be more accurate under certain conditions. One of the properties that FCT algorithms should have is that the density profile should be undisturbed if the flow velocity is zero. The SHASTA algorithm does not have this property, as can be seen by substituting $\epsilon = 0$ in the equations above. As a result, SHASTA suffers from residual damping in the Fourier domain at all wavelengths. One way to obtain zero residual damping when $\epsilon = 0$ is to use a form of the antidiffusive fluxes which exactly cancels the diffusion in Eq. (20). The transport and diffusive step in SHASTA LPE is identical to that for the SHASTA algorithm, except that SHASTA LPE uses

$$v_{i+1/2,j} = \tfrac{1}{6} + \tfrac{1}{3}\epsilon^2_{i+1/2,j}. \quad (22)$$

The form of the antidiffusive fluxes, though, is quite different,

$$A_{i+1/2,j} = \mu_{i+1/2,j}(x_{i+1} - x_i) \times [f^{\rm td}_{i+1,j} - f^{\rm td}_{i,j} - \tfrac{1}{6}(\Delta\rho_{i+1,j} - \Delta\rho_{i,j})], \quad (23a)$$

$$\Delta\rho_{i,j} = [(x_{i+1} - x_i)/\Delta x_i](f^{\rm td}_{i+1,j} - f^{\rm td}_{i,j}) - [(x_i - x_{i-1})/\Delta x_i](f^{\rm td}_{i,j} - f^{\rm td}_{i-1,j}), \quad (23b)$$

with

$$\mu_{i+1/2,j} = \tfrac{1}{6}(1 - \epsilon^2_{i+1/2,j}). \quad (23c)$$

This is called Pheonical antidiffusion because the undamped solution "rises whole from the ashes" as did the Phoenix.[18] The low-phase error (LPE) designation is used because v and μ have been chosen to minimize phase errors in the Fourier domain. One can see from Eq. (23) that part of the reason for the increased accuracy of this algorithm is that it uses information further away from the grid point being updated than the SHASTA algorithm uses. The SHASTA LPE method uses the one-sided limiter of Boris and Book, which is given by

$$A^c_{i+1/2,j} = S\max\{0,\min[S(f^{\rm td}_{i'+1,j} - f^{\rm td}_{i',j}),|A_{i+1/2,j}|]\}, \quad (24)$$

where $i' = i - S$ and $S = \text{sign}(f^{\rm td}_{i+1} - f^{\rm td}_i)$. This limiter is stronger than the one-sided limiter used by Zalesak.[17] That is, it allows less of the antidiffusive flux to flow.

For each of the three algorithms, the flux limiters were chosen to be as permissive as possible without introducing nonphysical results. This was done by performing a series of tests using different flux limiters in which an electron beam was propagated in the cathode fall without collisions. The results were then compared to the analytical solution. The optimum amount of flux limiting was found to be dependent on the degree of diffusiveness in the transport and diffuse step. Since the SHASTA LPE method is less diffusive and more dispersive than the DCM and SHASTA, the limiter used with it was stronger.

B. Collisional processes

After the transport step was completed, the time rate of change of the distribution function due to collisional processes was calculated. The rate of change in f due to inelastic collisional processes is

$$\left(\frac{\partial}{\partial t} f_{i,j}\right)_c = -\sum_\kappa (f_{i,j} v_j \sigma_{\kappa,j} N) + \sum_{m>j} \{f_{i,m} v_m \sigma_{\kappa,m} N \times \delta[v_m - (v_j + \Delta v_\kappa)]\}, \quad (25)$$

where $\sigma_{\kappa,j}$ is the cross section for process κ at velocity j, N is the neutral gas density, and Δv_κ is the change in velocity resulting from the inelastic collision. The second term in Eq. (25) represents the influx of electrons from inelastic collisions at higher velocities. In the case of an ionization an additional term for the secondary electron is added.

The electron momentum transfer cross section for helium used in this work was obtained from Hayashi[27] while the cross sections for excitation of He were obtained from Boeuf and Marode.[1] Their cross sections for excitation of the 2^1S, 2^3S, and 2^3P levels were combined into a single process with a threshold energy of 19.8 eV. Similarly, their cross sections for the 2^1P, $3SPD$, $4SPD$, and $5SPD$ levels were combined into a single process with a threshold energy of 21.25 eV. The ionization cross section and the distribution of secondary electrons were obtained from Green and Sawada.[28] These cross sections are shown in Fig. 2.

After the total rate of change of f at each grid point due to collisions was calculated, the distribution function was updated in time using the same Δt as in the transport step. A second-order predictor-corrector algorithm was used for the kinetics update. This completed a full time step in the calculation. BE was integrated in time in the cited fashion, after specifying initial and boundary conditions, until all values of $f(v_x,x)$ on the space-velocity mesh reached the steady state.

C. Monomodal and bimodal velocity representations

Anisotropic scattering is an important aspect of electron transport since it is this process which dominates momentum transfer at electron energies below the inelastic thresholds. In solving BE in regions of high E/N, such as in the cathode fall of glow discharges, methods which have assumed only forward scattering have been quite successful in obtaining inelastic collision rates.[13] The multibeam simulation is one such example.[10,11] Their success is a result of the fact that the electrons which are responsible for excitation and ionization are at a sufficiently high energy that their scattering is dominantly directed forward. Even though excitation processes are dominated by high-energy electrons, other transport coefficients, such as the drift velocity, are dominated by the more numerous low-energy secondary electrons away from the cathode. To accurately represent these coefficients, nonforward scattering must be accounted for.

Tran, Marode, and Johnson[13] modeled electron trajectories in the cathode fall using the Monte Carlo method while assuming only forward scattering. Boeuf and Marode[1]

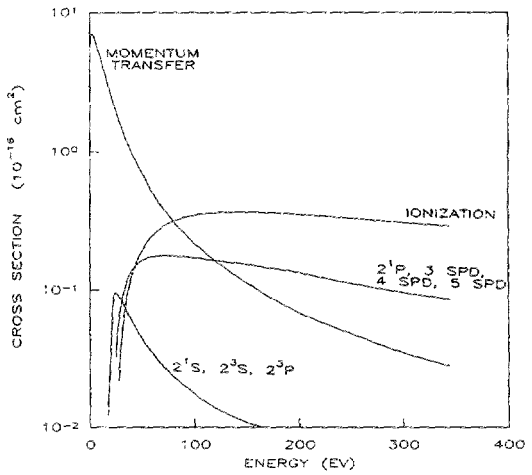

FIG. 2. Electron impact cross sections for helium used in this work. (See Refs. 1, 27, and 28).

repeated the calculation allowing fully anisotropic scattering. They found that including nonforward scattering processes gives rise to more low-energy electrons than a one-dimensional, forward scattering representation predicts. Boeuf and Marode concluded, however, that the essential features of electron behavior in the cathode fall may be determined using a one-dimensional model.

In our solution for the EVD in the cathode fall, two methods were used. The first, called the monomodal method, considers only positive (plasma directed) velocities, and therefore ignores nonforward scattering. The method is analogous to, and can be directly compared to multibeam or unidirectional Monte Carlo simulations. In order to accurately model nonforward scattering and momentum transfer, additional phase space dimensions are required. The second method we used approximates this by considering both positive and negative (cathode directed) velocity components. This technique, which we refer to as the bimodal method, enables us to include momentum transfer in a one-dimensional calculation. In the bimodal method, momentum transfer collisions are represented by the mixing of ^{+}v and ^{-}v velocity components so that when the rates of momentum transfer collisions are high, we obtain $f(^{+}v) \approx f(^{-}v)$, or an isotropic EVD. A forward beamlike velocity distribution would have $f(^{+}v)/f(^{-}v) \gg 1$. Momentum transfer and velocity mixing collisions are included in the collision integral as

$$\left(\frac{\partial f}{\partial t}(^{\pm}v)\right)_c = -0.5 N v \sigma_m(v)[f(^{\pm}v) - f(^{\mp}v)], \qquad (26)$$

where $v = |^{\pm}v|$ and σ_m is the momentum transfer cross section.

IV. COMPUTED ELECTRON VELOCITY DISTRIBUTIONS IN THE CATHODE FALL

In this section, we will present spatially dependent electron distributions obtained by directly integrating Boltzmann's equation as an initial value problem using flux corrected transport. As a demonstration of the method, and to facilitate comparison of this method with other established techniques for solving the spatially dependent BE, we have simulated the cathode fall region of a glow discharge in He. Comparisons are then made to multibeam and Monte Carlo simulations, and the effectiveness of the bimodal velocity approximation is discussed. We will also compare EVDs obtained using the three different FCT algorithms described in Sec. III.

A. Electron distribution in the cathode fall

The electron distribution in the cathode fall of a He discharge, obtained with the monomodal FCT model, is shown in Figs. 3 and 4. The cathode is at $x = 0$, the cathode fall voltage is $V_c = 150$ V, and the cathode fall extends to $d_c = 1.3$ cm. The gas pressure is 1 Torr at a temperature of 273 K, and the electric field is given by $E(x) = -2V_c(1 - x/d_c)/d_c$. The electric field in the negative glow is 1 V/cm and an absorbing anode for forward directed electrons is at $d_a = 1.5$ cm. The EVD was obtained by specifying an initial boundary condition for the electron

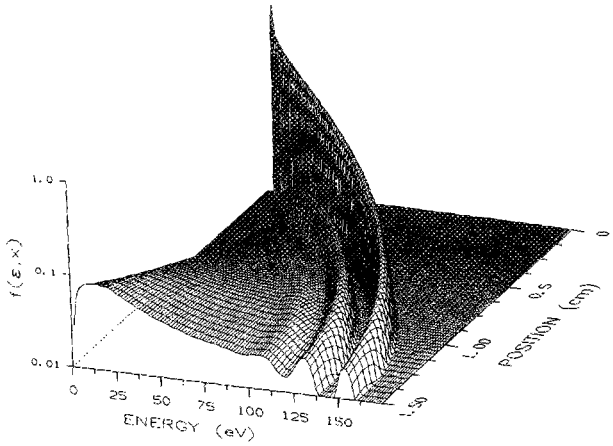

FIG. 3. Electron velocity distribution (EVD) as a function of distance from the electrode in the cathode fall of a glow discharge in helium. These results were obtained by direct integration of Boltzmann's equation using the monomodal velocity approximation and FCT algorithms. The normalization of the distribution is $eV^{-0.5}$ cm^{-1}, and the distribution is plotted using an energy axis for clarity. The cathode fall voltage is $V_c = 150$ V, cathode fall thickness is $d_c = 1.3$ cm, and the gas pressure is 1 Torr. Note the development of the beam component of the EVD and the dominance of secondary electrons near the end of the cathode fall.

flux at the cathode and directly integrating BE in time, using the methods described in Secs. II and III, until the distribution relaxed to its steady state. The boundary condition is that the electron flux emitted from the cathode is uniformly distributed between approximately 4 and 5 eV. For these results the DCM with FCT enhancements were used. The grid spacing in velocity space has points 1.5 eV apart in energy. The grid spacing in coordinate space has locations so that the electric potential changes by 1.5 V between points.

The characteristic features of electron distributions in the cathode fall[1,10-13] are obtained from this solution, as shown in Figs. 3 and 4. The beam component of the distribution follows a trajectory in the (ϵ,x) plane given by the electric potential. The density of electrons in the beam decreases across the cathode fall because of the increase in velocity (at constant flux) and because of the depletion resulting from collisions. When the beam energy reaches the first electronic excitation threshold (19.6 eV), a second group of beam electrons appears with an energy about 20 eV less than the local beam energy. These electrons have suffered one inelastic collision. When the beam electrons gain enough energy to cause ionizations (24.5 eV), a distribution of low-energy electrons develops from the influx of secondary electrons. Since the majority of secondary electrons are emitted with energies less than 20 eV, the first inelastic threshold, their rate of energy loss is small. By the end of the cathode fall, the electron distribution is dominated by the more numerous secondary electrons.

The fact that the calculated beam component of the distribution has a larger width, in energy, at the end of the cathode fall than the energy width of secondary electrons emitted from the cathode is a result, in part, of numerical diffusion. The numerical spreading of density from a single point when using the FCT method tends to be limited to only a few adjacent cells, typically 2–3, independent of the time of calculation or distance of convection. Using a low-order

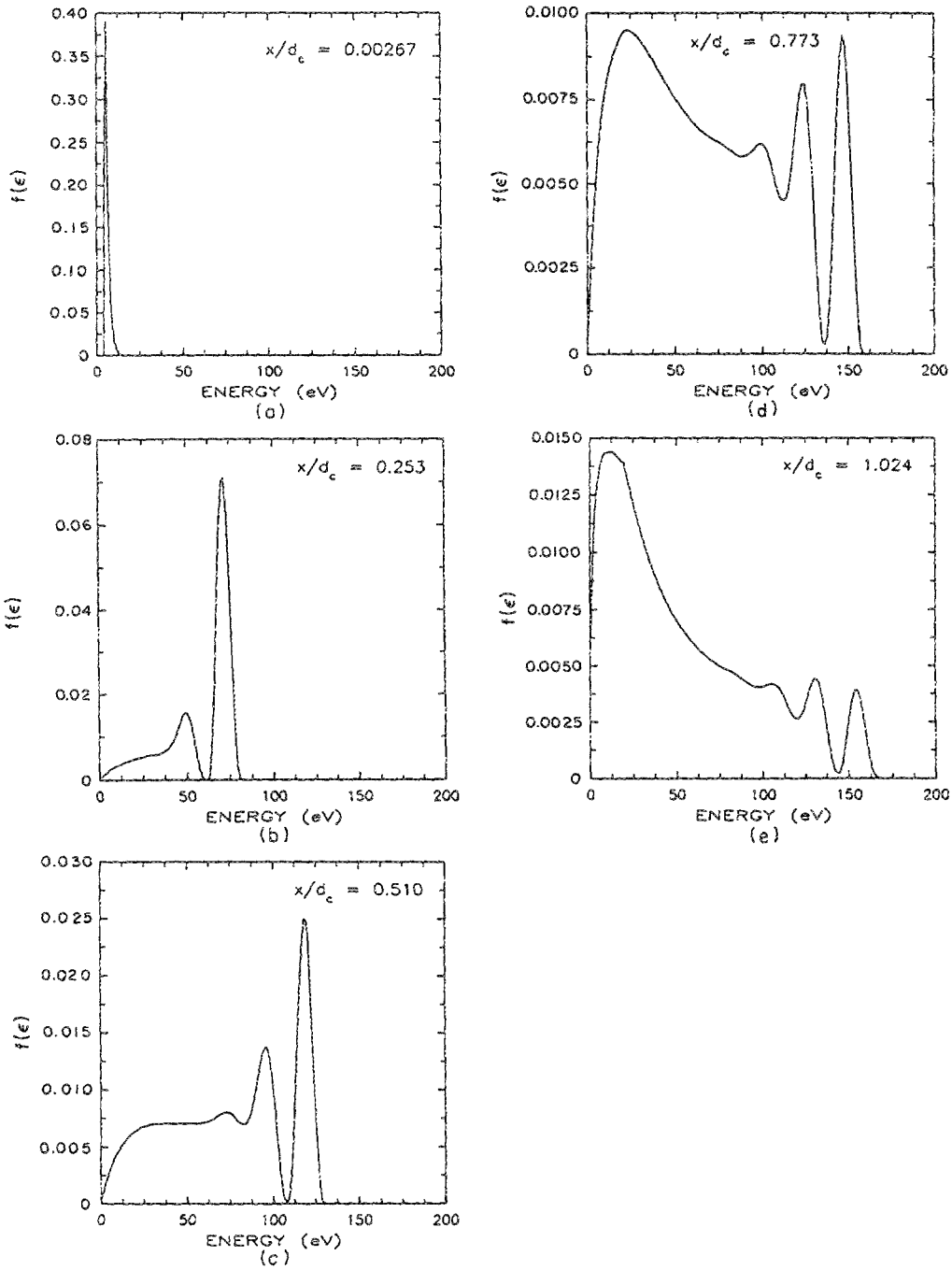

FIG. 4. Electron velocity distribution at various locations from the cathode for the condition of Fig. 3. The normalization of the distributions is $eV^{-0.5}$, and the distributions are plotted using an energy axis for clarity.

technique, such as the DCM, the spreading increases with increasing time or distance over conceptually an unlimited number of cells. Due to the steep gradient in electric potential in the cathode fall, a spreading in x space corresponds to a spread in potential energy. The spread in potential energy is ultimately transformed to a spread in kinetic energy as the cathode fall is traversed. The width of, for example, the beam component in phase space is therefore determined by the coarser of the spatial or velocity grids. Given this dependence, the optimum computational grid has cell widths in x- and v-space which have the same energy spacing (potential energy for x, kinetic energy for v).

The electron distribution in the cathode fall obtained using the bimodal velocity approximation for the same conditions as above is shown in Fig. 5. That portion of the distribution labeled with negative energy has ^{-}v velocities (i.e., moving towards the cathode); positive energy denotes ^{+}v trajectories (i.e., moving away from the cathode). The flux of secondary electrons emitted from the cathode is the same as that for the monomodal model. The boundary condition at the cathode is reflective with respect to the flux in the ^{-}v direction; $f(^{+}v,x=0)=f(^{-}v,x=0)$. At the anode the boundary condition is $f(^{-}v,x=d_a)=0$. Electrons in either half of the distribution are transferred to the other half at one half the rate of momentum transfer, as described by Eq. (26). Note the near absence of a cathode directed electron beam in Fig. 5. This results from the fact that the momentum transfer cross sections in He at energies exceeding tens of eV are low and there is a sparsity of secondary electrons emitted at energies exceeding 10–20 eV. At low energies (<10 eV),

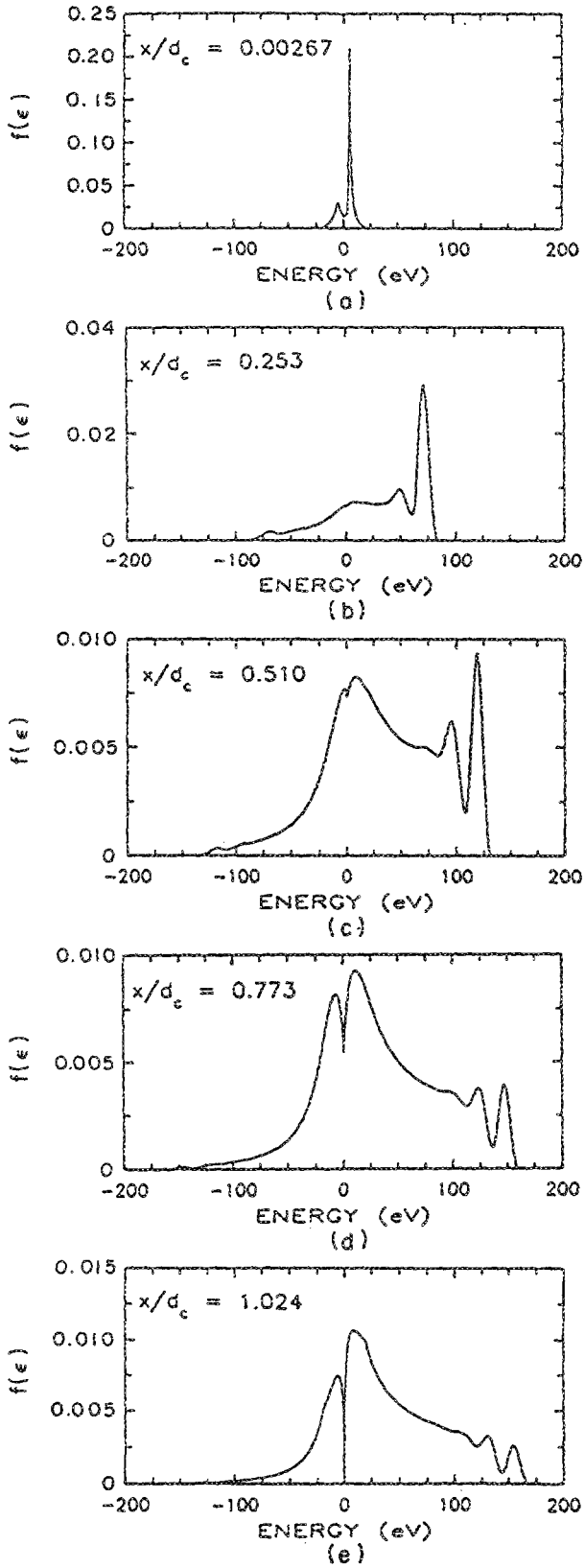

FIG. 5. Electron velocity distribution (EVD) obtained by directly integrating Boltzmann's equation using the bimodal velocity approximation and FCT algorithms. The EVDs are shown at different locations within the cathode fall, whose conditions are the same as in Fig. 3. The normalization of the distributions is $eV^{-0.5}$, and the distribution is plotted using an energy axis for clarity. Negative energy denotes trajectories moving towards the cathode; positive energy denotes trajectories moving away from the cathode. Note the absence of a cathode directed beam component, a consequence of the low rate of momentum transfer at energies exceeding tens of eV.

where the momentum transfer cross sections are large, the electron fluxes in the ^{-}v and ^{+}v components have nearly equal magnitudes, thereby yielding a nearly isotropic distribution.

To quantify the anisotropy of the distribution using the bimodal approximation, we define the parameter

$$\beta = \frac{2f(^{+}v)}{[f(^{+}v) + f(^{-}v)]} - 1. \tag{27}$$

A beamlike distribution directed away from the cathode has $\beta \approx 1$, an isotropic distribution has $\beta = 0$, and a beamlike distribution directed towards the cathode has $\beta \approx -1$. The anisotropy of the distribution as a function of electron energy at various positions in the cathode fall is shown in Fig. 6(a) for $V_c = 150$ V. The energy averaged anisotropy as a

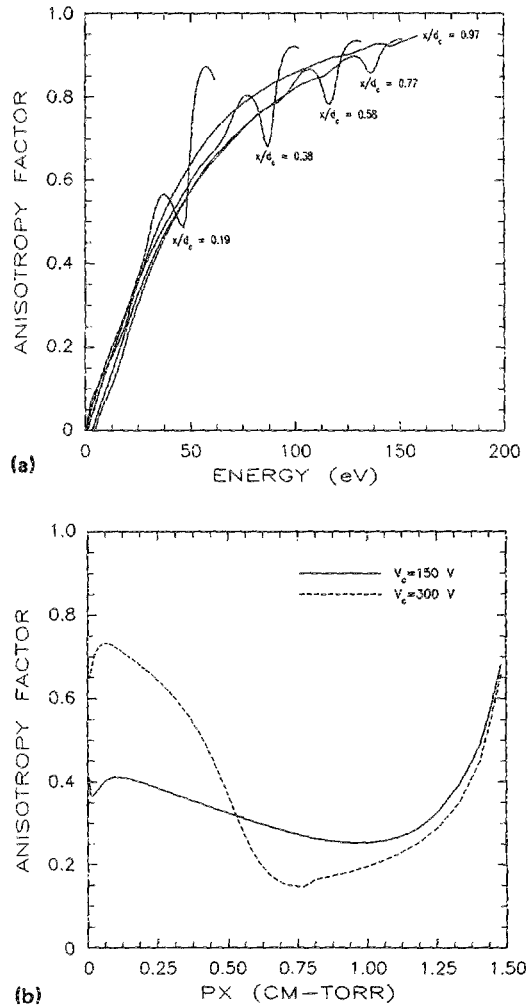

FIG. 6. Anisotropy factor β of the electron velocity distribution (EVD) obtained using the bimodal velocity approximation. $\beta = 1$ denotes an EVD which is beamlike in the forward direction (moving away from the cathode), $\beta = 0$ denotes an isotropic distribution and $\beta = -1$ denotes a beamlike EVD toward the cathode. (a) Anisotropy as a function of energy at various locations within the cathode fall for a voltage of $V_c = 150$ V. The limiting beamlike character of the EVD increases with increasing distance from the cathode. (b) Average anisotropy of the EVD as a function of position from the cathode for fall voltages of $V_c = 150$ and 300 V, and a gas pressure of 1 Torr. The decrease in the beamlike nature of the distribution is a result of the influx of secondary electrons; the increase results from the lack of cathode moving electrons near the anode of 1.5 cm.

function of position is shown in Fig. 6(b) for $V_c = 150$ V ($d_c = 1.3$ cm) and 300 V ($d_c = 0.8$ cm). The maximum anisotropy as a function of energy increases (that is, becomes more forward beamlike) as one moves away from the cathode since momentum transfer cross sections decrease with increasing electron energy, and the maximum available electron energy increases with distance from the cathode. For electron energies below tens of eV where momentum transfer cross sections are high, the distribution is fairly isotropic regardless of position. The distribution averaged anisotropy, as shown in Fig. 6(b), decreases with distance from the cathode up to the end of the cathode fall, and then becomes more beamlike near the anode. The decrease in anisotropy as one moves away from the cathode is a result of the buildup of secondary electrons which quickly thermalize due to their large momentum transfer cross sections. The forward directed beam component is simultaneously being depleted by collisions to lower energy where momentum transfer is higher. For our particular conditions, the distribution becomes more forward directed near the anode. This is a consequence of the boundary condition $f(\vec{v}, x = d_a) = 0$, which leaves only forward directed electrons near the anode. Note that the distribution for $V_c = 300$ V is both initially more beamlike, and later more isotropic. This behavior results from the fact that the momentum transfer cross sections are smaller for the more energetic beam obtained with $V_c = 300$ V, and so the distribution is initially more forward directed. The more energetic beam, however, has a higher rate of ionization and produces a larger relative influx of secondary electrons near the edge of the cathode fall. These secondary electrons quickly thermalize, thereby reducing the anisotropy.

B. Comparison between FCT algorithms

The application of this method to the solution of BE is subject to numerical effects which depend both on the computational mesh and the specifics of the FCT algorithms used. A comparison between EVDs at the boundary between the cathode fall and negative glow using the DCM, DCM with FCT correction, SHASTA FCT, and SHASTA LPE FCT algorithms appears in Fig. 7. The mesh spacing is the same for all examples. The DCM without FCT does not preserve any of the structure of the distribution at high energies, a result of excessive numerical diffusion. The SHASTA and DCM FCT algorithms give nearly identical results, whereas the SHASTA LPE algorithm preserves the beamlike structure more accurately. It is, however, more sensitive to variations in the flux limiters. The larger value of the distribution in the high-energy peaks yields a slightly higher rate of ionization, resulting in a slightly larger relative density of secondary electrons at low energy. The increased accuracy comes at only a few percent increase in the computation time.

The EVD at the end of the cathode fall is shown in Fig. 8 for $V_c = 150$ V using two different grid resolutions. The solid curve was obtained using a 1.5-eV separation between mesh points, while the dashed curve was obtained using 0.75 eV per mesh point. The beam portion of the distribution is narrower and the underlying structure is better resolved us-

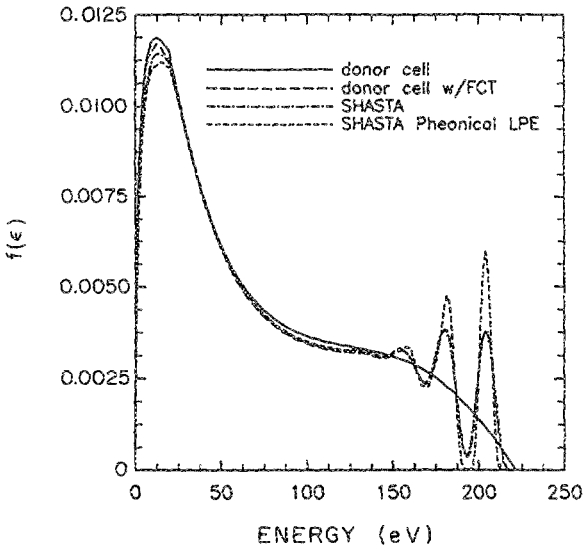

FIG. 7. Comparison of electron velocity distributions in the cathode fall ($V_c = 200$ V) using the low-order donor cell method (DCM) without flux corrected transport (FCT), and three different FCT algorithms. The mesh spacing is the same for all cases. The normalization of the EVDs is $eV^{-0.5}$, plotted with an energy axis for clarity. The low-order DCM is unable to preserve any of the high-energy structure of the beam component; the SHASTA LPE method is most accurate in that regard.

ing the finer mesh, as one would expect. Since the method is conservative, the integral of the beam component is the same in each method and the distribution averaged quantities are not significantly different. The resolved peaks are a result of successive energy losses of 20 eV for electronic excitation and 25 eV for ionization. At low energy this structure is buried below the secondary electron distribution[11] and the difference between the two grids is small. This exercise demonstrates the ability of the FCT technique to resolve detailed features with a reasonable number of mesh points. Obtaining

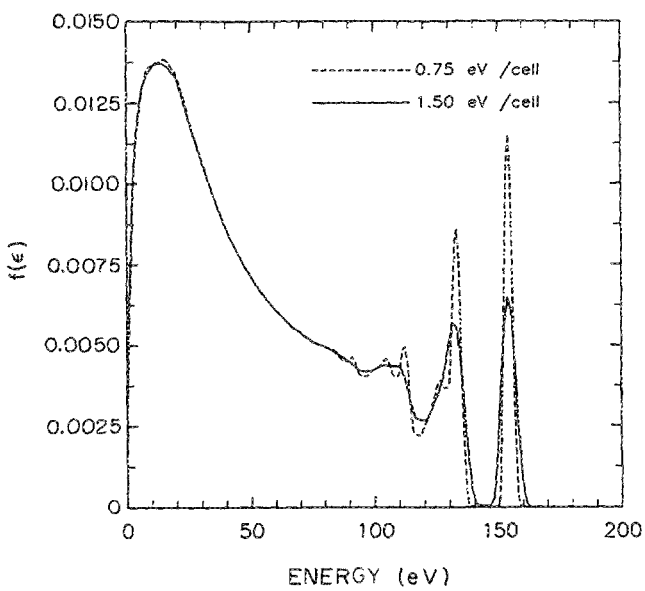

FIG. 8. The electron velocity distribution for the conditions of Fig. 3 using two grid resolutions: 1.5 and 0.75 eV/cell.

an equivalent resolution using conventional lower-order techniques, such as the DCM without FCT, would require 5–10 times the number of mesh points, and proportionally more computer time.

C. Comparisons with Monte Carlo simulations and multibeam models

In this section, comparisons are made between our solution of Boltzmann's equation using FCT and conventional solutions in order to validate our method. Comparisons are made to the Monte Carlo simulations of Boeuf and Marode (BM),[1] Tran and co-workers,[13] and to the multibeam model of Carman and Maitland.[10] In the simulation by Tran, only forward scattering is allowed, which is equivalent to the monomodal FCT model. In the simulation by Boeuf and Marode, full angular scattering is included, which may be compared to the bimodal approximation.

The electron convective drift velocity or average velocity $v_d = \langle \mathbf{v} \rangle$ and ionization coefficient α as a function of position for $V_c = 150$ V are shown in Fig. 9 using the FCT monomodal and bimodal models. These are compared to the results of the Tran and BM simulations. The ionization coefficient is defined as $\alpha = k_I/v_d$, where k_I ($\mathrm{cm^3\ s^{-1}}$) is the rate coefficient for electron impact ionization. The results from the monomodal FCT model and the forward scattering Monte Carlo simulation of Tran agree well for both drift velocity and ionization coefficient, thereby validating the FCT method for these conditions. Near the cathode the electrons are accelerated by the field but do not decelerate by collisions until they reach the inelastic threshold energy, and thus the convective drift velocity increases. As lower-energy secondary electrons begin to dominate the distribution, and the beam component is depleted, the convective drift velocity decreases.

The convective drift velocity obtained with the bimodal FCT initially agrees with the Monte Carlo simulation of BM using full angular scattering, but diverges near the edge of the cathode fall. The qualitative behavior, though, is similar. The convective drift velocity is smaller than that obtained with the monomodal models due to the influx of secondary electrons which quickly thermalize to a smaller *net* velocity and which dominates the distribution near the edge of the cathode fall. (A fully isotropic distribution would have $v_d = 0$.) The increase in convective drift velocity near the anode (at $d_a = 1.5$ cm) is a consequence of the boundary condition $f(\vec{v}, x = d_a) = 0$. The lack of cathode directed electrons near the anode leaves dominantly forward directed electrons, thereby increasing the *net* velocity. The average velocity obtained using fully anisotropic elastic scattering in the BM simulation is lower than that obtained using the bimodal FCT model. Conceptually, having off-axis components of velocity in the BM simulation keeps electrons in a given spatial region longer than in the bimodal FCT. Therefore their local rates of collision are higher, momentum transfer more complete, and average velocity lower. Because the convective drift velocity is lower in the BM simulation, the ionization coefficient is higher than that obtained from the bimodal FCT model even though the number of net ionizations is virtually the same in each case. This is an artifact

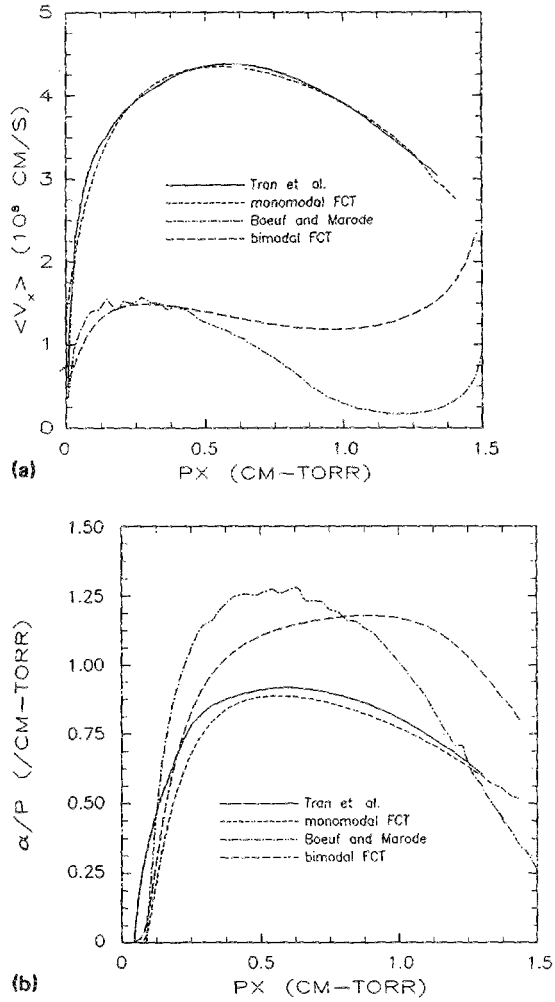

FIG. 9. Transport coefficients obtained from our solution of Boltzmann's equation using the monomodal and bimodal approximations with FCT algorithms: (a) Convective drift velocity and (b) ionization coefficient α. The cathode fall voltage is 150 V. Comparisons are made to the Monte Carlo simulations of Tran and co-workers (Ref. 13), and Boeuf and Marode (Ref. 1). The bimodal solution and the Monte Carlo simulation using full angular scattering (Boeuf and Marode) predict lower convective drift velocities due to the high isotropy of the secondary electrons. The high value of α for the nonforward directed solutions results partly from their lower convective drift velocities.

of the definition of α, which is inversely proportional to v_d.

The multibeam method of Carman and Maitland[10] is a one-spatial-dimension model which calculates the energy distribution of the electron flux. In the multibeam model, the forward directed flux at position x and energy ϵ, $j(\epsilon,x)$ is obtained from

$$j(\epsilon - eE(x)\delta x, x + \delta x) = j(\epsilon,x)\exp(-N\sigma_T(\epsilon)\delta x) + \left(\sum_i \int_{\epsilon}^{\epsilon\phi(x)} j(\epsilon',x)\sigma_i(\epsilon')N\delta[\epsilon' - (\epsilon + \Delta\epsilon_i)]\,d\epsilon'\right)\delta x, \tag{28}$$

where ϕ is the local electrical potential, E is the electric field, σ_T is total cross section for inelastic energy loss, and σ_i is the cross section for loss of energy $\Delta\epsilon_i$ for process i. The terms of Eq. (28) are for depletion of a beamlet by collisions, and for the influx of electrons to the beamlet from collisions at high-

er energy. An additional term is added for the influx of secondary electrons from ionizations. Numerical effects are minimized by precisely choosing $\Delta\epsilon = \Delta x(eE)$.

The flux multiplication factor $j_e(x)/j_e(0)$ and average flux energy obtained with the monomodal FCT method are compared to the results of Carman and Maitland in Fig. 10 for four different cathode fall voltages. The two methods agree fairly well. A flux multiplication of 2–3 is typical for cathode falls in He and this result is obtained by each method. The average flux energy initially increases due to the distribution being dominated by the beam component. The average flux energy then decreases as the beam is depleted and the distribution begins to be dominated by low-energy secondary electrons. The fraction of the cathode fall voltage obtained by the average flux energy increases with increasing V_c. This effect is a result of the cross sections for inelastic energy loss having their maximum values at $\lesssim 150$ eV. When this value is exceeded, the beam component persists. This effect is more clearly seen in Fig. 11 where the electron flux distributions obtained using the FCT algorithms at the boundary between the cathode fall and negative glow are plotted for increasing cathode fall voltage.

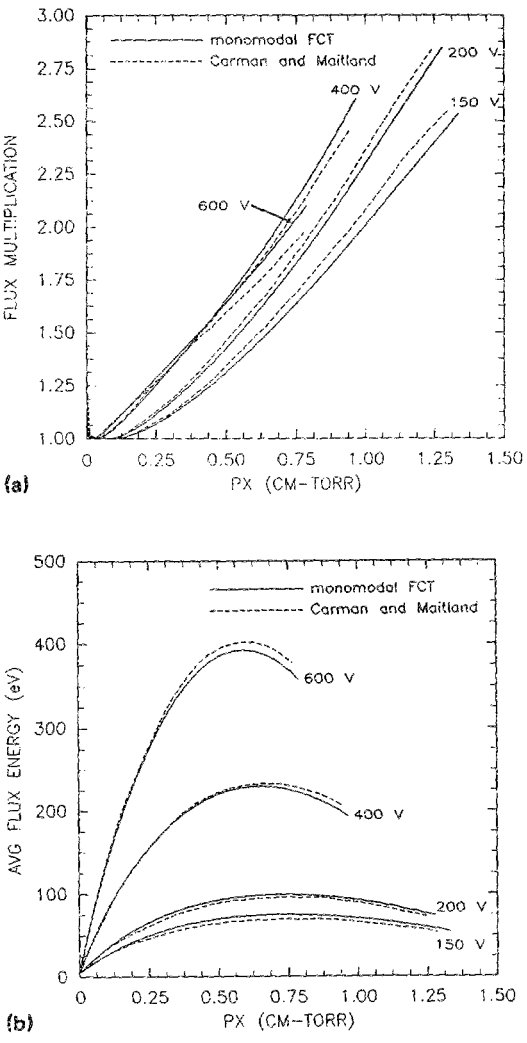

FIG. 10. Comparison of results from the monomodal FCT model and the multibeam method of Carman and Maitland (Ref. 10) for different cathode fall voltages V_c: (a) flux multiplication, $j(x)/j(x=0)$ and (b) average flux energy.

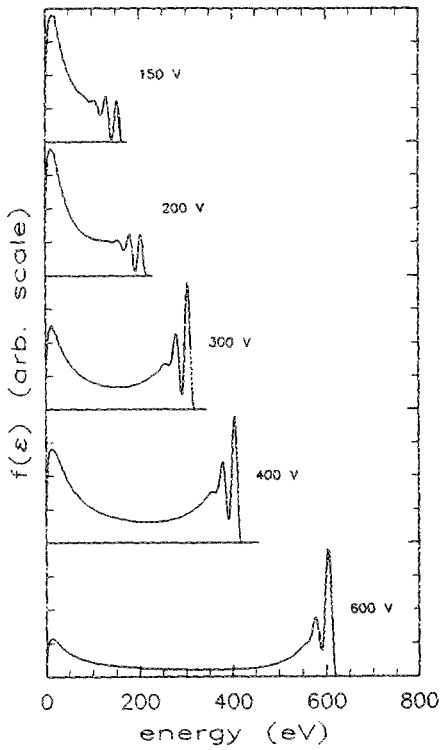

FIG. 11. Electron flux distributions at the boundary between the cathode fall and negative glow in helium obtained using the monomodal FCT algorithms. Distributions are shown for increasing cathode fall voltages V_c.

V. CONCLUDING REMARKS

The application of flux corrected transport (FCT) to direct integration of the spatially dependent Boltzmann's equation (BE) for the electron velocity distribution using finite differences has been investigated. Directly integrating BE has the advantage of being an exact solution, subject to constraints on dimensionality, but suffers from mechanical inaccuracies such as numerical diffusion. The use of FCT alleviates many of the effects of numerical diffusion. The electron distributions obtained by this method agree well with other computational techniques using the monomodal representation. The transport properties obtained using the FCT method incorporating the bimodal velocity approximation closely resemble those obtained using the fully anisotropic Monte Carlo simulation of Boeuf and Marode.[1] The agreement with other computational techniques and with experimental results is more dependent on the physical assumptions of the model, such as scattering mechanisms, rather than on any conceptual limitations of the method.

Using FCT to integrate Boltzmann's equation eliminates many of the detriments of using finite differences or variances thereof. In particular, the mesh may have arbitrary spacings, which is not the case in the multibeam implementation. The greatest limitation of the method, however, is the restriction on the time step set by the Courant limit.[26] Although the FCT algorithms do require more operations per time step than standard finite difference methods, the

FCT algorithms usually execute faster. This is a result of the fact that the number of mesh points required to obtain a given resolution is much smaller than in, for example, the DCM. The use of fewer, more widely spaced mesh points, also corresponds to a larger Courant limited time step, thereby further increasing the speed of the algorithm. When steady-state spatially dependent electron distribution functions at low gas pressure and high voltage are desired, the small time step dictated by the Courant limit may make other algorithms more attractive, such as Monte Carlo simulations or the convective scheme of Sommerer, Hitchon, and Lawler.[12] At higher pressures and with transients in the electric field, methods which directly integrate BE, such as that presented here, may be preferred.

ACKNOWLEDGMENTS

The authors would like to thank Professor P. F. Williams (University of Nebraska) and Dr. R. Carman (Maquarie University) for their advice on the topic of this paper. This work was supported by Sandia National Laboratory and the National Science Foundation (CBT 88-03170 and ECS 88-15781).

[1]J. P. Boeuf and E. Marode, J. Phys. D **15**, 2169 (1982).
[2]D. A. Doughty, E. A. Den Hartog, and J. E. Lawler, Phys. Rev. Lett. **58**, 2668 (1987).
[3]P. Gill and C. E. Webb, J. Phys. D **10**, 299 (1977).
[4]R. Winkler, M. Dilonardo, M. Capitelli, and J. Wilhelm, Plasma Chem. Plasma Proc. **7**, 125 (1987).
[5]R. A. Gottscho, Phys. Rev. A **36**, 2233 (1987).
[6]M. J. Kushner, J. Appl. Phys. **54**, 4958 (1983).
[7]G. L. Braglia, J. Wilhem, and R. Winkler, Nuovo Cimento **80**, 21 (1984).
[8]A. V. Phelps and L. C. Pitchford, Phys. Rev. A **31**, 2932 (1985).
[9]K. Kitamori, H. Tagashira, and Y. Sakai, J. Phys. D **11**, 283 (1978).
[10]R. J. Carman and A. Maitland, J. Phys. D **20**, 1021 (1987).
[11]B. Shi, G. J. Fetzer, Z. Yu, J. D. Meyer, and G. J. Collins, IEEE J. Quantum Electron. **QE-25**, 948 (1989).
[12]T. J. Sommerer, W. N. G. Hitchon, and J. E. Lawler, Phys. Rev. A **39**, 6356 (1989).
[13]N. A. Tran, E. Marode, and P. C. Johnson, J. Phys. D **10**, 2317 (1977).
[14]B. N. Ganguly, M. R. Shoemaker, B. L. Preppernau, and A. Garscadden, J. Appl. Phys. **61**, 2778 (1987).
[15]E. A. Den Hartog, D. A. Doughty, and J. E. Lawler, Phys. Rev. A **38**, 2471 (1988).
[16]J. P. Boris and D. L. Book, J. Comput. Phys. **11**, 38 (1973).
[17]S. T. Zalesak, J. Comput. Phys. **31**, 335 (1979).
[18]J. P. Boris and D. L. Book, in *Methods in Computational Physics*, edited by J. Killeen (Academic, New York, 1976), p. 85.
[19]J. P. Boris and D. L. Book, J. Comput. Phys. **20**, 397 (1976).
[20]J. P. Boris, D. L. Book, and K. Hain, J. Comput. Phys. **18**, 248 (1975).
[21]R. Morrow and L. E. Cram, J. Comput. Phys. **57**, 129 (1985).
[22]E. E. Kunhardt and C. Wu, J. Comput. Phys. **68**, 127 (1987).
[23]R. Morrow, Phys. Rev. A **32**, 1799 (1985).
[24]S. K. Dhali and P. F. Williams, J. Appl. Phys. **62**, 4696 (1987).
[25]S. K. Dhali and A. K. Pal, J. Appl. Phys. **63**, 1355 (1988).
[26]The Courant limit on the integrating time step is $\Delta t_{\max} = \min[(\Delta x_j/v_j),(\Delta v_k/a_k)]$, where Δx and Δv are the mesh spacings on the spatial and velocity grids, and v and a are the velocity and acceleration.
[27]M. Hayashi, *Recommended Values of Transport Cross Sections for Elastic Collision and Total Collision Cross Section for Electrons in Atomic and Molecular Gases*, Report No. IPPJ-AM-19 (Nagoya Institute of Technology, 1982).
[28]A. E. S. Green and T. Sawada, J. Atmos. Terr. Phys. **34**, 1719 (1972).